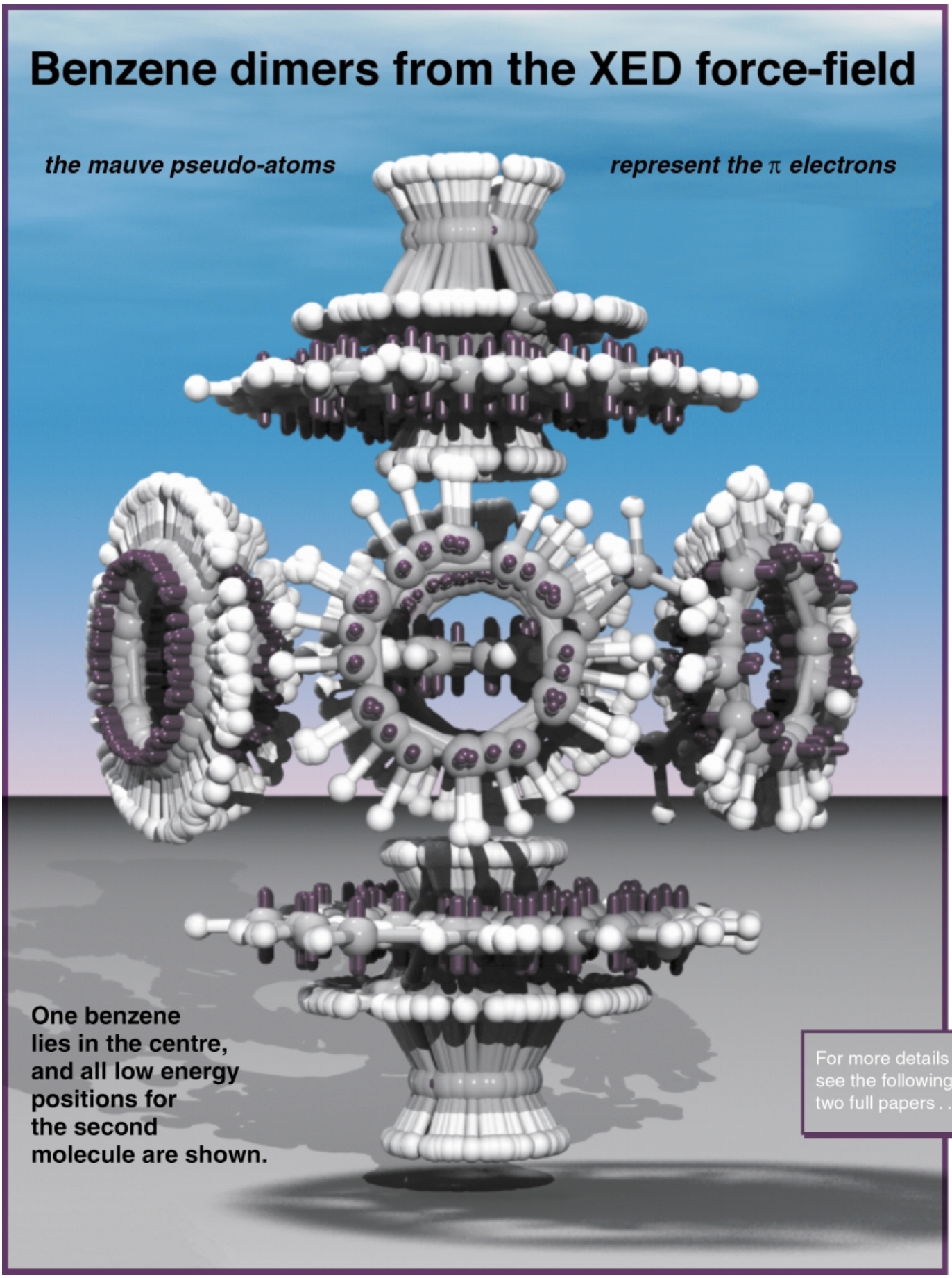

  0947-6539/02/0813-2847 $ 20.00+.50/0

Substituent Effects on Edge-to-Face Aromatic Interactions

Fiona J. Carver,[a] Christopher A. Hunter,*[a] David J. Livingstone,[b] James F. McCabe,[a] and Eileen M. Seward[c]

Abstract: Chemical double mutant cycles have been used to measure the magnitude of edge-to-face aromatic interactions in hydrogen-bonded zipper complexes as a function of substituents on both aromatic rings. The interaction energies vary depending on the combination of substituents from $+1.0$ kJ mol^{-1} (repulsive), to -4.9 kJ mol^{-1} (attractive). The results correlate with the Hammett substituent constants which indicates that electrostatic interactions are responsible for the observed differences in interaction energy. The experiments can be rationalised based on local electrostatic interactions between the protons on the edge ring and the π-electron density on the face ring as well as global electrostatic interactions between the overall dipoles on the two aromatic groups.

Keywords: host–guest systems · pi interactions · supramolecular chemistry

Introduction

Intermolecular interactions are sensitive to solvent, orientation and substituents. In order to experimentally probe the basic chemistry which governs weak non-covalent interactions, we require systems where one of these parameters can be changed without affecting anything else. Synthetic supramolecular systems provide the ideal solution for developing structure–activity relationships for understanding intermolecular interactions.[1] Simple dipole interactions such as H-bonding have been understood for a long time,[2] but aromatic interactions are more complicated, and have proved more difficult to study.[3] Despite a number of structure–activity studies of aromatic interactions in supramolecular systems, a consistent picture has not yet emerged. Diederich found that electron withdrawing substituents increased the affinity of naphthalene derivatives for an aromatic macrocycle.[4] Siegel and Cozzi have shown that electron withdrawing substituents generally stabilise aromatic stacking interactions.[5] However, if the quadrupole of one of the groups is reversed by perfluorination, then electron donating substituents are required in the other ring to produce a favourable interaction.[6] These experiments suggest that electrostatic interactions are important in determining the magnitudes of aromatic interactions: increasing the electrostatic complementarity of the molecular surfaces leads to a more favourable interaction. In contrast, Wilcox found no evidence for significant electrostatic interactions in edge-to-face aromatic interactions in his torsion balance and concluded that van der Waals interactions were more important.[7] We have been studying aromatic interactions in H-bonded zipper complexes using chemical double mutant cycles.[8] In this paper, we show how the approach has been used to construct a structure–activity relationship for edge-to-face aromatic interactions.

[a] Prof. C. A. Hunter, Dr. F. J. Carver, Dr. J. F. McCabe
Centre for Chemical Biology
Krebs Institute for Biomolecular Science
Department of Chemistry, University of Sheffield
Sheffield S3 7HF (UK)
Fax: (+44) 114-273-8673
E-mail: c.hunter@sheffield.ac.uk

[b] Dr. D. J. Livingstone
ChemQuest, Delamere House, 1 Royal Crescent, Sandown
Isle of Wight PO36 8LZ (UK)

[c] Dr. E. M. Seward
Merck Sharp & Dohme Research Laboratories
Neuroscience Research Centre, Terlings Park
Eastwick Road, Harlow, Essex CM20 2QR (UK)

Results and Discussion

To begin, we decided to investigate the influence of nitro, hydrogen and dimethylamino substituents on both the edge and the face ring of the edge-to-face aromatic interaction in complex A (Scheme 1): this represents more or less the full range of polarising effects which are accessible from strongly electron withdrawing through neutral to strongly electron donating and allows us to assess whether the thermodynamic consequences are large enough to detect. Both *para* and *meta* substituents were studied on the edge ring, since this change in isomer introduces a significant difference in the geometry of the aromatic interaction. Only *para* substituents were consid-

  0947-6539/02/0813-2848 $ 20.00+.50/0

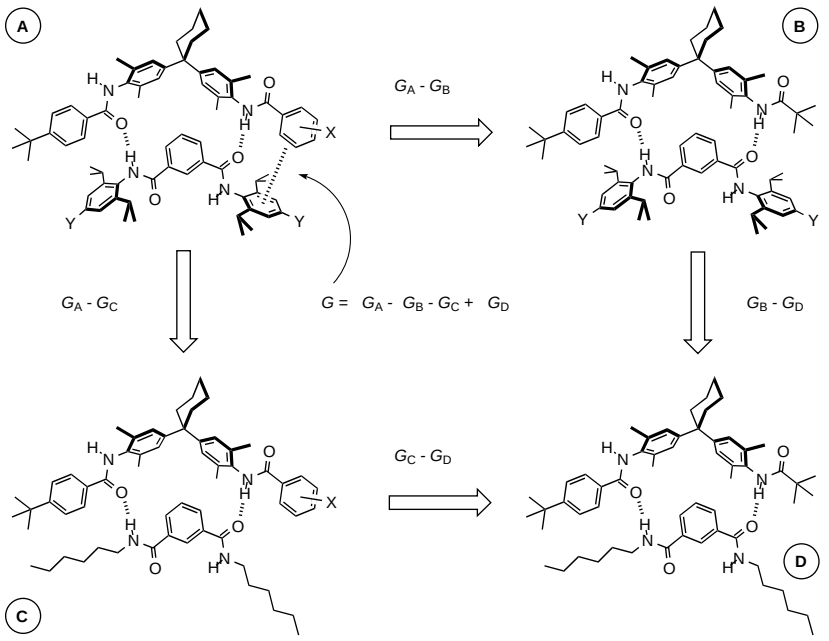

Scheme 1. A chemical double mutant cycle for determining the magnitude of the terminal aromatic interaction in complex A. Y = NO_2, H, NMe_2. X = *p*-NO_2, *m*-NO_2, H, *p*-*t*Bu, *p*-NMe_2, *m*-NMe_2.

ered on the face ring, because *meta* substituents would clash with the neighbouring isopropyl group. In addition, the *p*-*tert*-butyl group on the edge ring was investigated, since compound **1** was already available in our laboratory.[8a]

Synthesis: The compounds required to construct the chemical double mutant cycles in Scheme 1 were prepared according to Schemes 2 and 3. Compounds **1**–**6** have been reported previously.[9] Simple amide coupling reactions were used to prepare compounds **7**–**11** from **6**, and with the exception of the synthesis of **11** which was not optimised, the reactions proceeded in good yield. The introduction of substituents on 2,6-diisopropylaniline was achieved according to literature procedures.[10] After protection of the amine as the tosylate, **14** was selectively nitrated at the *para* position to give **15** (protection as the acetate led to nitration at the *meta* position). Compound **15** was deprotected with sulphuric acid to give the desired *p*-nitroaniline, **16**. However, the coupling of **16** with isophthaloyl chloride to give **12** proved rather difficult. The combination of the severe steric hindrance and the electron withdrawing effects of the *p*-nitro substituent make **16** a poor nucleophile, and the only conditions which produced any of the coupling product were prolonged refluxing in dry pyridine with 4-(dimethylamino)-pyridine. The corresponding *p*-dimethylaminoaniline (**19**) was prepared by reducing the protected *p*-nitroaniline, **15**, followed by reductive methylation and deprotection with sulphuric acid. **19** coupled readily with isophthaloyl dichloride to give **13**.

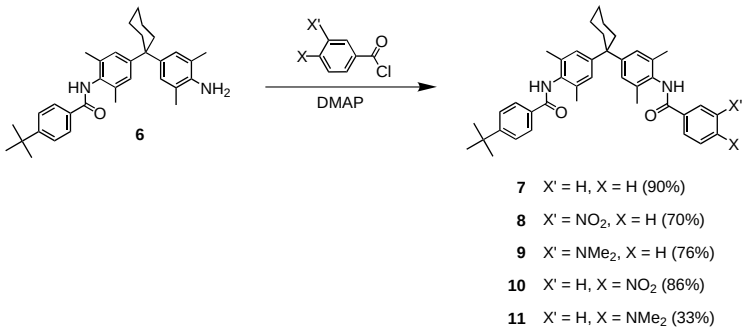

Scheme 2. Synthesis of complexes **7**–**11**.

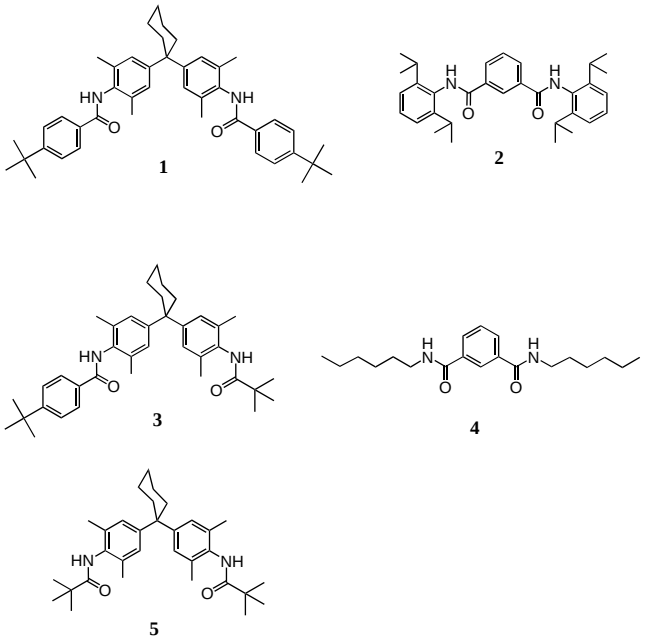

NMR Binding studies: The complexes formed by these compounds were characterised using ^{1}H NMR titration experiments, and the results are summarised in Tables 1–3. For some of the weak binding complexes only 50% saturation was achieved, and in general, this can lead to errors in the association constant determined by curve fitting due to uncertainty in extrapolation of the limiting complexation-induced change in chemical shift ($\Delta\delta$).[11] However in these systems, the $\Delta\delta$ values are consistent across the whole range of complexes which indicates there are no problems in the extrapolation for the weak binding complexes. The association constants show a significant dependence on the nature of the substituents X and Y (Table 1). For complex A which contains the aromatic interaction of interest, the values range from 8 M^{-1} when X = *m*-NMe_2 and Y = NMe_2 to 240 M^{-1} when X = *p*-NMe_2 and Y = NO_2. The range of values observed for the control complexes, B, C and D (which involve compounds

Table 1. Association constants (K_a in M^{-1}) measured from ^1H NMR titrations in deuterochloroform at 295 K.[a]

			Bisaniline compound							
Isophthaloyl compound	**Y**	**X**:	**11** *p*-NMe_2	**9** *m*-NMe_2	**1** *t*Bu	**7** H	**10** *p*-NO_2	**8** *m*-NO_2	**3** –	**5** –
13	NMe_2		18 ± 1	8 ± 1	19 ± 1	22 ± 1	126 ± 5	52 ± 4	8 ± 1	6 ± 1
2	H		47 ± 2	23 ± 2	48 ± 2	43 ± 1	170 ± 6	80 ± 2	17 ± 1	12 ± 1
12	NO_2		240 ± 30	122 ± 8	123 ± 9	122 ± 5	120 ± 6	126 ± 9	79 ± 4	47 ± 1
4	–		17 ± 1	12 ± 1	15 ± 1	14 ± 2	25 ± 3	26 ± 2	10 ± 1	10 ± 1

[a] Average values from at least three separate experiments. Titration data for 4–6 different signals were used to determine the association constant in each experiment. Errors are quoted as twice the standard error from the weighted mean (weighting based on the observed change in chemical shift).

Table 2. Free energies of complexation (ΔG in kJ mol^{-1}) measured from ^1H NMR titrations in deuterochloroform at 295 K.[a]

			Bisaniline compound							
Isophthaloyl compound	**Y**	**X**:	**11** *p*-NMe_2	**9** *m*-NMe_2	**1** *t*Bu	**7** H	**10** *p*-NO_2	**8** *m*-NO_2	**3** –	**5** –
13	NMe_2		– 7.1 ± 0.2	– 4.9 ± 0.3	– 7.2 ± 0.2	– 7.6 ± 0.1	– 11.8 ± 0.1	– 9.9 ± 0.2	– 4.9 ± 0.3	– 4.4 ± 0.4
2	H		– 9.4 ± 0.1	– 7.8 ± 0.1	– 9.5 ± 0.1	– 9.2 ± 0.1	– 12.6 ± 0.1	– 10.7 ± 0.1	– 6.9 ± 0.1	– 6.0 ± 0.2
12	NO_2		– 13.4 ± 0.3	– 11.7 ± 0.2	– 11.8 ± 0.2	– 11.7 ± 0.1	– 11.7 ± 0.5	– 11.7 ± 0.2	– 10.7 ± 0.1	– 9.5 ± 0.1
4	–		– 6.9 ± 0.1	– 6.0 ± 0.2	– 6.6 ± 0.2	– 6.5 ± 0.4	– 7.9 ± 0.3	– 8.0 ± 0.2	– 5.6 ± 0.3	– 5.6 ± 0.3

[a] Average values from at least three separate experiments. Titration data for 4–6 different signals were used to determine the association constant in each experiment. Errors are quoted as twice the standard error from the weighted mean (weighting based on the observed change in chemical shift).

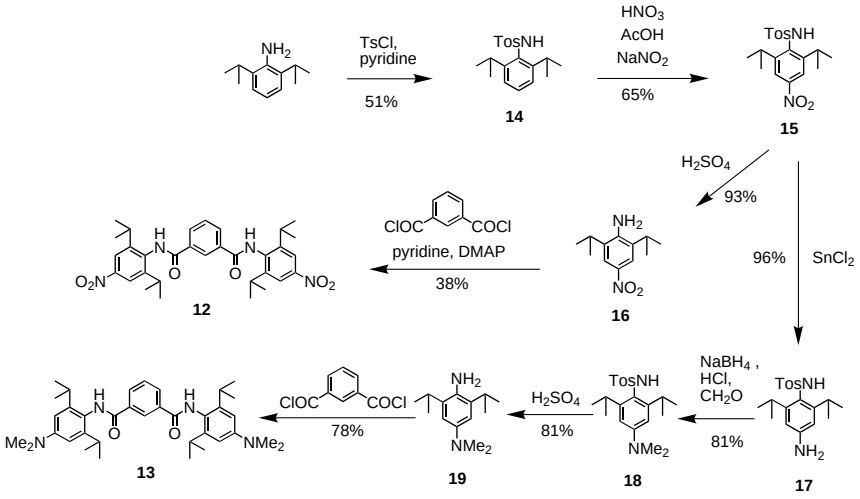

Scheme 3. Synthesis of compounds **12** and **13**.

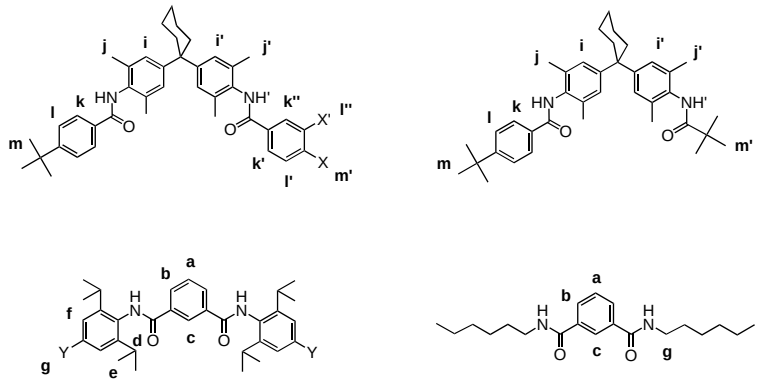

Scheme 4. Proton assignment.

they contain a nitroaromatic interaction or not. This implies that one effect of the nitro groups is to increase the strength of the H-bonding interactions by polarising the amide NHs.

Structures of the complexes: Information about the three-dimensional structures of the complexes was obtained from the limiting complexation-induced changes in chemical shift for formation of a 1:1 complex ($\Delta\delta$ values in Table 3) and intermolecular NOEs observed in two-dimensional ROESY experiments (Figure 1, Table 4). The $\Delta\delta$ values in Table 3 are remarkably similar for all of the 32 complexes, implying that the range of chemical mutations used does not have a dramatic effect on the three-dimensional structure of the complexes. The isophthaloyl signals **a** and **b** show large upfield shifts which indicates that they sit over the face of an aromatic ring, while the other isophthaloyl signal **c** is unaffected by complexation which indicates that it sits on the outside of the complex. The small downfield change in chemical shift observed for the bisaniline aromatic protons **i** and **i′** suggest that they sit on the edge of an aromatic ring and that the isophthaloyl group is docked into the bisaniline

3, **4** and **5** in Table 1) are smaller, but they are significant which highlights the importance of the double mutant approach. For example, all of the complexes which contain nitro groups show enhanced stability regardless of whether

0947-6539/02/0813-2850 $ 20.00+.50/0 *Chem. Eur. J.* **2002**, *8*, No. 13

Table 3a. Limiting complexation-induced changes in ^{1}H NMR chemical shift ($\Delta\delta$ in ppm) from NMR titrations in deuterochloroform at 295 K.[a]

				Isophthaloyl compound						
Complex	**X**	**Y**	**NH**	**a**	**b**	**c**	**d**	**e**	**f**	**g**
	complex A									
11·13	*p*-NMe_2	NMe_2	+0.8	−1.1	−0.3	0.0	0.0	−0.1	0.0	0.0
11·2	*p*-NMe_2	H	+1.3	−1.6	−0.4	0.0	0.0	−0.1	0.0	0.0
11·12	*p*-NMe_2	NO_2	+1.7	−1.4	−0.3	0.0	0.0	−0.2	−0.1	–
9·13	*m*-NMe_2	NMe_2	+1.3	−1.3	−0.5	+0.1	−0.1	−0.1	+0.2	0.0
9·2	*m*-NMe_2	H	+1.3	−1.4	−0.3	+0.1	−0.1	−0.2	0.0	0.0
9·12	*m*-NMe_2	NO_2	+1.6	−1.3	−0.3	+0.1	−0.1	−0.2	−0.1	–
1·13	*p*-*t*Bu[b]	NMe_2	+1.3	−1.3	−0.3	0.0	0.0	−0.1	0.0	0.0
1·2	*p*-*t*Bu[b]	H	+1.4	−1.6	−0.4	0.0	0.0	−0.2	0.0	+0.1
1·12	*p*-*t*Bu[b]	NO_2	+1.9	−1.4	−0.3	+0.1	0.0	−0.2	−0.1	–
7·13	H	NMe_2	+1.1	−1.2	−0.3	0.0	0.0	−0.1	0.0	0.0
7·2	H	H	+1.3	−1.6	−0.4	0.0	0.0	−0.1	0.0	0.0
7·12	H	NO_2	+1.4	−1.3	−0.3	0.0	0.0	−0.2	0.0	–
10·13	*p*-NO_2	NMe_2	+1.1	−1.5	−0.5	0.0	−0.1	−0.1	0.0	+0.1
10·2	*p*-NO_2	H	+1.2	−1.7	−0.5	0.0	−0.1	−0.2	0.0	+0.1
10·12	*p*-NO_2	NO_2	+1.6	−1.3	−0.4	0.0	0.0	−0.2	0.0	–
8·13	*m*-NO_2	NMe_2	+1.0	−1.4	−0.4	0.0	−0.1	−0.2	0.0	0.0
8·2	*m*-NO_2	H	+1.1	−1.5	−0.4	0.0	−0.1	−0.2	−0.1	0.0
8·12	*m*-NO_2	NO_2	+1.4	−1.5	−0.4	0.0	−0.1	−0.2	−0.1	–
	complex B									
3·13	–	NMe_2	+1.0	−1.5	−0.4	0.0	0.0	−0.1	0.0	0.0
3·2	–	H	+1.4	−1.7	−0.6	0.0	−0.1	−0.2	−0.1	0.0
3·12	–	NO_2	+1.6	−1.5	−0.4	0.0	0.0	−0.1	−0.1	–
	complex C									
11·4	*p*-NMe_2	–	+0.9	−0.7	−0.3	0.0	–	–	–	−0.3
9·4	*m*-NMe_2	–	+0.9	−1.0	−0.1	0.0	–	–	–	−0.3
1·4	*p*-*t*Bu[b]	–	+1.1	−0.7	−0.2	0.0	–	–	–	−0.3
7·4	H	–	+0.8	−0.7	−0.2	0.0	–	–	–	−0.3
10·4	*p*-NO_2	–	+0.7	−0.8	−0.3	0.0	–	–	–	−0.3
8·4	*m*-NO_2	–	+0.7	−0.8	−0.4	0.0	–	–	−0.3	
	complex D									
3·4	–	–	+1.0	−0.8	−0.4	0.0	–	–	–	−0.3
	complexes with **5**[c]									
5·13	–	NMe_2	+0.6	−0.9	−0.3	0.0	0.0	0.0	0.0	0.0
5·2	–	H	+1.1	−1.5	−0.4	0.0	0.0	0.0	0.0	0.0
5·12	–	NO_2	+1.5	−1.5	−0.5	0.0	0.0	−0.1	0.0	–
5·4	–	–	+0.7	−0.7	−0.4	0.0	–	–	–	−0.2

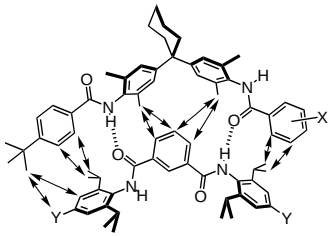

Figure 1. Intermolecular NOEs observed in ROESY experiments on 1:1 mixtures of the components of the complexes A (Table 4).

pocket in an edge-to-face geometry. All of the amide NH signals experience downfield shifts indicating that they are involved in H-bonding interactions. In complex A which contains the edge-to-face aromatic interaction of interest, the protons on the edge ring, **k**, **k′**, **l** and **l′**, all show significant upfield complexation-induced changes in chemical shift which confirms that they lie over the face of a nearby aromatic ring. The small upfield shifts observed for the isopropyl methyl signals of the isophthaloyl compound in complex A are consistent with this edge-to-face geometry: the methyl groups lie over the face of the benzoyl ring which is docked into the groove between them on the face of the aniline ring. The $\Delta\delta$ values for the **1·2** complex have been used previously to derive a complete three-dimensional structure which confirms this interpretation of the chemical shift data.[12] Unambiguous intermolecular NOEs were observed for all 12 complex A molecules (Table 4, Figure 1). Although not all of the NOEs in Figure 1 were observed for every complex, the pattern of NOEs is the same for all 12 complexes and is consistent with the three-dimensional structure shown in Scheme 1. The isophthaloyl group is close to the bisaniline pocket, and there are close contacts between the terminal aromatic rings involved in the edge-to-face interactions.

The general pattern of $\Delta\delta$ values in Table 3 is the same for all of the complexes, but there are some differences that are worth noting. For example, the $\Delta\delta$ values for the isophthaloyl signals **a** and **b** are consistently smaller in complexes C and D compared with complexes A and B (Table 3a). We have shown previously that these differences are due to increased flexibility of the isophthaloyl group within the bisaniline pocket, when the steric buttressing of the aniline rings is removed.[9c] In other words, this represents a very minor structural change, and since it occurs in two complexes in the double mutant cycle (C and D), any thermodynamic effects cancel out when all four complexes in the cycle are considered.

Table 3b. Limiting complexation-induced changes in ^{1}H NMR chemical shift ($\Delta\delta$ in ppm) from NMR titrations in deuterochloroform at 295 K.[a]

			Bisaniline compound													
Complex	**X**	**Y**	**NH**	**i**	**j**	**k**	**l**	**m**	**NH′**	**i′**	**j′**	**k′**	**l′**	**m′**	**k″**	**l″**
	complex A															
11·13	*p*-NMe_2	NMe_2	+1.2	+0.2	+0.2	−0.1	−0.4	−0.1	+1.6	+0.2	+0.2	−0.3	−0.3	−0.2	–	–
11·2	*p*-NMe_2	H	+1.1	+0.2	−0.2	−0.2	−0.1	0.0	+0.8	+0.2	nd	−0.1	−0.2	−0.1	–	–
11·12	*p*-NMe_2	NO_2	+0.3	+0.2	0.0	−0.3	−0.4	−0.1	+1.0	+0.2	−0.1	−0.5	−0.4	−0.1	–	–
9·13	*m*-NMe_2	NMe_2	nd	+0.2	0.0	−0.2	−0.3	−0.1	nd	+0.2	0.0	−0.1	−0.3	−0.1	−0.1	−0.2
9·2	*m*-NMe_2	H	nd	+0.1	−0.1	−0.1	−0.3	0.0	nd	+0.1	−0.1	−0.1	0.0	−0.2	nd	−0.2
9·12	*m*-NMe_2	NO_2	+0.4	nd	−0.1	−0.2	−0.2	−0.1	+0.4	+0.1	nd	−0.2	nd	−0.1	nd	−0.2
1·13	*p*-*t*Bu[b]	NMe_2	+1.2	+0.2	0.0	−0.2	−0.4	−0.1	+1.2	+0.2	0.0	−0.2	−0.4	−0.1	–	–
1·2	*p*-*t*Bu[b]	H	+1.1	+0.2	0.0	−0.3	−0.5	−0.1	+1.1	+0.2	0.0	−0.3	−0.5	−0.1	–	–
1·12	*p*-*t*Bu[b]	NO_2	+0.6	+0.2	0.0	−0.3	−0.4	−0.1	+0.6	+0.2	0.0	−0.3	−0.4	−0.1	–	–
7·13	H	NMe_2	+1.6	+0.2	0.0	−0.2	nd	−0.1	+1.6	+0.2	0.0	−0.2	nd	nd	–	–
7·2	H	H	nd	+0.1	0.0	−0.2	nd	0.0	+0.7	nd	0.0	−0.2	nd	nd	–	–
7·12	H	NO_2	+0.5	+0.1	0.0	−0.2	nd	−0.1	+0.3	nd	0.0	−0.2	nd	nd	–	–
10·13	*p*-NO_2	NMe_2	+0.4	+0.3	0.0	−0.5	−0.4	−0.1	+2.6	+0.2	+0.1	+0.1	−0.6	–	–	–
10·2	*p*-NO_2	H	+0.4	+0.2	0.0	−0.5	−0.4	−0.1	+2.4	+0.3	+0.1	0.0	−0.6	–	–	–
10·12	*p*-NO_2	NO_2	+0.3	+0.3	+0.1	−0.8	−0.6	−0.2	+2.4	nd	0.0	−0.1	−0.7	–	–	–
8·13	*m*-NO_2	NMe_2	+0.3	+0.2	0.0	−0.4	−0.4	−0.1	+2.1	+0.2	−0.1	−0.3	−0.5	0.0	−0.1	–
8·2	*m*-NO_2	H	+0.4	+0.1	0.0	−0.4	−0.5	0.0	+1.8	+0.1	0.0	−0.1	−0.9	−0.2	0.0	–
8·12	*m*-NO_2	NO_2	+0.2	+0.1	0.0	−0.5	−0.4	−0.1	+2.3	+0.2	0.0	−0.1	−0.3	−0.2	−0.1	–
	complex B															
3·13	–	NMe_2	+1.1	+0.2	−0.2	−0.1	−0.4	−0.1	+0.7	+0.2	0.0	–	–	−0.2	–	–
3·2	–	H	+0.9	+0.2	−0.1	−0.2	−0.4	0.0	+0.6	+0.2	0.0	–	–	−0.2	–	–
3·12	–	NO_2	+0.4	nd	−0.1	−0.3	−0.3	−0.1	nd	+0.1	−0.3	–	–	−0.2	–	–
	complex C															
11·4	*p*-NMe_2	–	+1.0	0.0	−0.1	+0.1	0.0	−0.2	+0.6	nd	−0.1	+0.3	0.0	0.0	–	–
9·4	*m*-NMe_2	–	+0.9	0.0	−0.1	0.0	−0.1	0.0	+0.9	0.0	−0.1	+0.1	0.0	0.0	nd	−0.1
1·4	*p*-*t*Bu[b]	–	+0.9	0.0	−0.1	−0.1	−0.1	0.0	+0.9	0.0	−0.1	−0.1	−0.1	0.0	–	–
7·4	H	–	+1.2	0.0	−0.1	+0.1	−0.1	0.0	+1.2	0.0	−0.1	+0.1	nd	nd	–	–
10·4	*p*-NO_2	–	+1.0	+0.1	−0.2	+0.1	0.0	0.0	+2.0	0.0	0.0	+0.2	−0.1	–	–	–
8·4	*m*-NO_2	–	+1.2	+0.1	−0.2	0.0	0.0	0.0	+2.2	−0.1	−0.1	+0.2	−0.1	−0.1	+0.3	–
	complex D															
3·4	–	–	+1.3	0.0	−0.2	−0.1	−0.1	0.0	+1.1	0.0	−0.1	–	–	0.0	–	–
	complexes with **5**[c]															
5·13	–	NMe_2	–	–	–	–	–	–	+0.5	0.0	−0.2	–	–	−0.3	–	–
5·2	–	H	–	–	–	–	–	–	+0.9	+0.1	0.0	–	–	−0.2	–	–
5·12	–	NO_2	–	–	–	–	–	–	+0.4	+0.1	−0.1	–	–	−0.3	–	–
5·4	–	–	–	–	–	–	–	–	+0.6	0.0	−0.1	–	–	0.0	–	–

[a] Calculated by extrapolating titration data for formation of 1:1 complexes. See Scheme 4 for the proton labelling scheme. Dashes indicate signals that do not exist in the complex concerned. nd represents data that was not determined due to signal overlap. [b] When X = *t*Bu, the bisaniline compound (**1**) is symmetrical, so **NH**, **i**–**m** are equivalent to **NH′**, **i′**–**m′**, and the data are listed as two sets of identical values. [c] Compound **5** is symmetrical, and **NH**, **i**–**m** do not exist in this molecule, so the data are recorded as one set of values, **NH′**, **i′**, **j′** and **m′**, according to the labels in Scheme 4.

Table 4. Intermolecular NOEs observed in two-dimensional ROESY experiments in deuterochloroform at 295 K.[a]

			Bisaniline compound					
Isophthaloyl compound	**Y**	**X**:	**11** *p*-NMe_2	**9** *m*-NMe_2	**1** *p*-*t*Bu[b]	**7** H	**10** *p*-NO_2	**8** *m*-NO_2
13	NMe_2					**a**–**j**		
			b–**j**,**j′**	**b**-**j**,**j′**	**b**-**j**	**b**-**j**,**j′**	**b**-**j**,**j′**	**b**-**j**,**j′**
			e–**k**,**l**		**e**-**k**,**l**	**e**-**k**,**k′**,**l**	**e**-**k**,**k′**,**l**	**e**-**k′**,**l**,**l′**
			f–**m**	**f**–**m**	**f**,**g**–**m**			**g**–**m**
2	H		**a**–**j**,**j′**		**a**–**j**			
			b–**j**,**j′**	**b**–**j**,**j′**	**b**–**j**	**b**–**j**,**j′**	**b**-**j**,**j′**	**b**-**j**,**j′**
			e–**k**,**k′**,**l**		**e**–**k**,**l**	**e**-**k**,**k′**,**l**,**l′**	**e**–**k**,**k′**,**l**,**l′**	**e**–**k**,**k′**,**l′**
			f–**m**		**f**,**g**–**m**	**g**–**m**		
12	NO_2		**b**–**j**	**b**–**j**,**j′**	**b**–**j**	**b**–**j**,**j′**	**b**–**j**,**j′**	**b**–**j**,**j′**
				e–**k**	**e**–**k**,**l**	**e**–**k**,**k′**	**e**–**k′**	
			f–**m**	**f**–**m**	**f**–**m**	**f**–**m**		

[a] Experiments were carried out on 1:1 mixtures of the two components at the maximum concentration possible (1–10 mM). See Scheme 4 for the proton labelling scheme and Figure 1 for a generalised illustration of the intermolecular NOEs in complex A. [b] For X = *t*Bu, the bisaniline compound (**1**) is symmetrical, so the two sides of the molecule are equivalent. Only one set of NOEs is recorded, but **j′**, **k′**, **l′** and **m′** are equivalent to **j**, **k**, **l**, and **m**, respectively.

0947-6539/02/0813-2852 $ 20.00+.50/0 *Chem. Eur. J.* **2002**, *8*, No. 13

The signals that show the greatest variation in $\Delta\delta$ values are those due to the amide protons. This is in part due to the fact that the changes are much larger for these signals and that the chemical shifts of signals due to H-bonded protons are dramatically altered by small changes in geometry, but in some cases, the very large differences observed appear to reflect a significant structural change. The complexes formed with compounds **10** and **8** provide the clearest examples. The $\Delta\delta$ value for **NH′** is approximately double that observed for the other systems, while the value for the bisaniline **NH** is unusually small (Table 3b). There are several possible explanations (for $X = NO_2$):

1) The hydrogen bond is stronger (as the K_a values in Table 1 suggest) and therefore shorter, and this change in geometry has a significant effect on the $\Delta\delta$ value;
2) the amide proton is more easily polarised which makes in the chemical shift of the proton more sensitive to electric field effects;
3) there is a change in the position of the equilibrium between the α and β conformers depicted in Scheme 5.

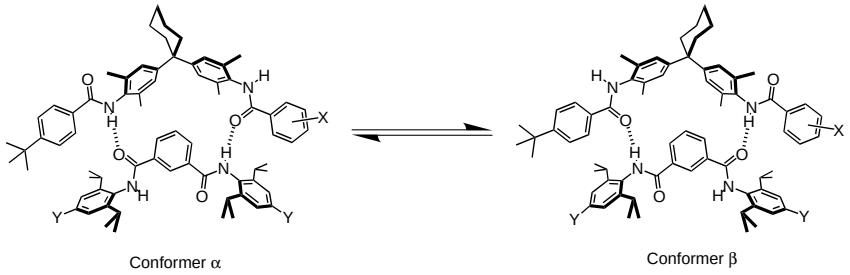

Scheme 5. Conformational equilibrium in unsymmetrical complexes.

The difference between conformers α and β is the orientation of the amide groups and H-bonds (see Scheme 5). This leads to a subtle difference in the orientation of the interaction between the terminal functional groups. Conformer α involves the edge ring carbonyl oxygen as the hydrogen-bond acceptor and the face ring NH as the H-bond donor. Conformer β involves the edge ring NH as the H-bond donor and the face ring carbonyl oxygen as the H-bond acceptor.

Although the other effects may play some role, the last explanation is clearly the most appealing, since it also accounts for the reduction in the $\Delta\delta$ value for the **NH** signal on the other side of the molecule. The presence of the two conformers in Scheme 5 and the significance for the double mutant analysis was discussed previously.[8, 9, 13] However, the systems described here provide an excellent probe of the $\alpha-\beta$ equilibrium: in conformer α, the bisaniline **NH** is hydrogen bonded and **NH′** is not, whereas in conformer β, **NH′** is hydrogen bonded and the bisaniline **NH** is not, and this will be reflected in the corresponding $\Delta\delta$ values. For most of the complexes, the$\Delta\delta$ values for the bisaniline **NH** and **NH′** are comparable which indicates roughly equal amounts of conformer α and β are present. However, when $X = NO_2$, conformer α becomes significantly more stable. This could be caused by a difference between the strengths of the terminal aromatic interactions in the two conformers, but the most plausible explanation is that the electron withdrawing effect of the nitro group makes **NH′** a much stronger hydrogen-bond donor than **NH**. Thus the double mutant cycles for the $X = NO_2$ systems really measure the interaction in conformer α, whereas the other interactions are measured as a population-weighted average of the two different conformers.

On closer examination of the $\Delta\delta$ values for the protons on the terminal aromatic rings, **k**, **k′**, **l** and **l′**, the change in the geometry of the complex from the α to the β conformer is clearly visible (Table 3b). In general in complex A, the $\Delta\delta$ values for **k** and **k′** and for **l** and **l′** are comparable, but the magnitudes of the upfield shifts are slightly larger for **l** and **l′**. However, when $X = NO_2$, a completely different pattern is observed. The values for the two sides of the molecule are no longer the same: $\Delta\delta$ for **k′** is close to zero; **l′** shows a large negative change; **k** and **l** show smaller negative $\Delta\delta$ values, but the change for **k** is slightly larger than for **l**. This pattern compares well with the $\Delta\delta$ values calculated previously for the **1·2** complex (Figure 2). The experimentally observed $\Delta\delta$ values for the **1·2** complex were used to determine a three-dimensional structure, and this process involved calculation of theoretical $\Delta\delta$ values for every individual proton in the complex and then averaging the symmetry-related values.[12] Thus, we can look at predicted $\Delta\delta$ values for lower symmetry complexes (Figure 2, $R \neq R'$). The pattern of predicted $\Delta\delta$ values is precisely that observed for the $X = NO_2$ complexes, and if we average across the complex (i.e., make $R = R'$), we obtain the pattern observed for the other complexes in which conformers α and β are present in equal amounts. The theoretical chemical shift calculation also helps with the interpretation of these values. In particular, why is the value for **k′** $+0.1$ ppm in Figure 2 even though it sits above the face of an aromatic ring? Although there is a ring current contribution of -0.3 ppm to the $\Delta\delta$ value for **k′** (which is the average of the values for the two equivalent **k′** protons), there is an even larger positive contribution of $+0.4$ ppm which comes from the electric field and anisotropy of the nearby amide carbonyl group. Thus, the $\Delta\delta$ values observed for **k′** when $X = NO_2$ indicate that there is a close contact between **k′** and the carbonyl oxygen which could represent a CH–O hydrogen-bonding interaction (Figure 2).

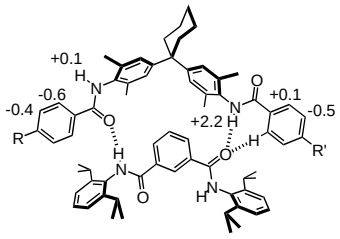

Figure 2. Calculated complexation-induced changes in ^{1}H NMR chemical shift for unsymmetrical complexes fixed in conformation β.[12] The positive $\Delta\delta$ value calculated for proton **k′**, is due to close proximity to the carbonyl group which is suggestive of the CH–O hydrogen bond shown.

The one major problem which becomes apparent from the data in Table 3b is the behaviour of the X = *m*-NMe_2 systems in complex A. An additional conformational equilibrium is possible for these complexes: in the In conformer, the *meta* substituent is folded onto the face of the aniline ring, and in the Out conformer, it is directed away from the complex (Scheme 6). Significant upfield shifts are observed for the signals due to the dimethylamino protons, **l″**. In addition, the $\Delta\delta$ values for **k′** and **l′** are rather small which suggests that the X = *m*-NMe_2 complex spends a significant amount of time in the In conformation. When X = *m*-NO_2, there is no ^{1}H NMR probe at position **l″**, but the large upfield shifts observed for **l′** suggest that the In conformer is not significantly populated. The interaction energy measured by the double-mutant cycle is therefore a weighted average of the In and Out conformers for the X = *m*-NMe_2 systems. Since the In conformer features a different interaction, an NMe – π interaction, these double-mutant cycles are not very meaningful. Although this does not occur for the X = *m*-NO_2 systems, there is a related problem, because the In conformer is not blocked by the hexyl chains in complex C. In principle, the $\Delta\delta$ values for **k′** and **k″** should give an indication of the relative populations of the In and Out conformers, but the magnitudes of the chemical shift changes are rather small. The value for **k″** is slightly larger in complex C, while the values for **k′** are slightly larger in complex A. This suggests that complex C populates both conformers, while complex A exists mainly as the In conformer. To account for this difference, we must modify the double-mutant cycle equation by adding a statistical term to allow for the two-fold difference in symmetry between complexes A and C:

$$\Delta\Delta G(m\text{-X}) = \Delta G_A - \Delta G_B - \Delta G_C + \Delta G_D - RT\ln 2 \quad (1)$$

Strictly, the statistical factor used here should reflect the ratio of the In and Out conformers in complexes A and C, but this can not be measured accurately, and given the chemical shift data above, a value of two seems to be a reasonable estimate.

Indirect evidence for the geometry of the aromatic interactions in these complexes can be obtained from model compounds as explained previously.[14] The packing of simple aromatic amides in the crystalline state gives rise to the same hydrogen bonds and edge-to-face interactions found in the solution complexation studies discussed above. Thus, the behaviour of the model compounds shown in Figure 3a) in the solid state gives us some insight into the effect of different substituents on the geometry of the terminal aromatic interaction in complex A in solution. Figure 3b) shows an overlay of dimers taken from the X-ray crystal structures of seven model compounds for which we have been able to obtain suitable quality single crystals. Clearly the geometry of the aromatic interaction is unaffected by changing the substituents on the two aromatic rings, and this provides further weight to the assertion that the geometry of complex A is insensitive to the nature of X and Y. The steric interactions associated with the *meta* substituted edge rings make them unsuitable for X-ray studies, since the model compounds crystallise as linear H-bonded polymers with edge-to-face interactions on both sides of each aromatic ring.

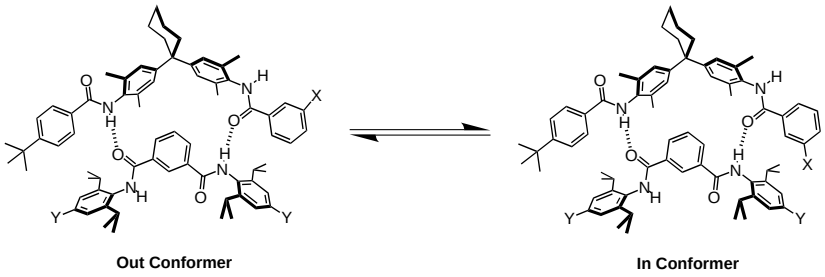

Scheme 6. Conformational equilibrium for *meta*-substituted edge rings. The substituent X can face into or out of the complex, and this affects the nature of the interaction that the double mutant cycle measures.

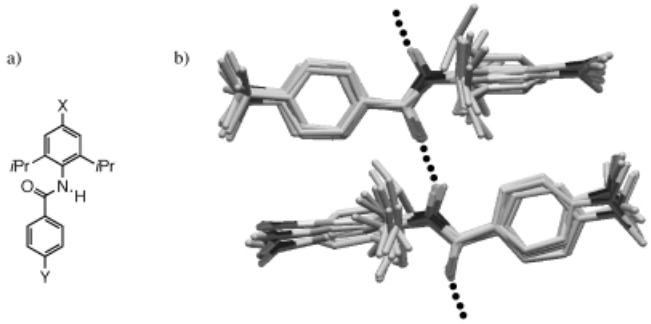

Figure 3. a) Model compounds used to probe the geometry of the aromatic interactions in the solid state as a function of substituent (X = NO_2, Y = *t*Bu; X = NO_2, Y = NMe_2; X = H, Y = NO_2; X = H, Y = *t*Bu; X = H, Y = NMe_2; X = NMe_2, Y = *t*Bu; X = NMe_2, Y = NMe_2). b) An overlay of dimers found in the X-ray crystal structures of these compounds.[13]

Experimental determination of edge-to-face aromatic interaction energies: These experiments show that this is a suitable system for a structure – activity study using the double mutant cycle approach. For all 32 complexes, the key functional groups have the same relative position and orientation, and any subtle structural changes that take place occur in a pairwise fashion for two components of the double-mutant cycle. Using the data in Table 2 and the double mutant cycle in Scheme 1, the magnitude of the terminal edge-to-face aromatic interaction in complex A was calculated as a function of X and Y. The results are summarised in Table 5. Although many of the values are similar (the same within the experimental error), there is a substantial spread from $+1.2\ kJ\,mol^{-1}$ to $-4.6\ kJ\,mol^{-1}$ which is equivalent to an order of magnitude in the binding constant. The method clearly allows us to quantify both repulsive and attractive intermolecular interactions. When X = Y = *p*-NO_2, the aromatic interaction is unfavourable. Although the precise values

  0947-6539/02/0813-2854 $ 20.00+.50/0 *Chem. Eur. J.* **2002**, *8*, No. 13

Table 5. Aromatic interaction energies ($\Delta\Delta\delta G$ in kJ mol^{-1}) in deuterochloroform at 295 K measured using the double mutant cycle in Scheme 1.

	p-X				*m*-X		
Y	NMe_2	*t*Bu	H	NO_2	NMe_2[a]	H	NO_2
NMe_2	-0.9 ± 0.5	-1.3 ± 0.5	-1.8 ± 0.6	-4.6 ± 0.5	-1.6 ± 0.5	-1.8 ± 0.6	-4.3 ± 0.5
H	-1.1 ± 0.4	-1.6 ± 0.4	-1.4 ± 0.5	-3.4 ± 0.4	-2.0 ± 0.4	-1.4 ± 0.5	-3.1 ± 0.4
NO_2	-1.4 ± 0.5	-0.1 ± 0.4	-0.2 ± 0.5	$+1.2\pm0.6$	-2.4 ± 0.4	-0.2 ± 0.5	-0.5 ± 0.4

[a] These results are not reliable because this system is complicated by the in/out conformational equilibrium illustrated in Scheme 5.

of the aromatic interaction energy are probably not directly transferable to other systems which may have a different geometry, combinations of functional groups or solvent, the data in Table 5 does provide a useful qualitative guide to the trends that might be expected and the size of potential thermodynamic effects. For example, if $X = NMe_2$, the interaction energy is insensitive to the nature of the face ring, but if $X = NO_2$, dramatic changes in the interaction energy can be achieved by changing the substituents (Y) on the face ring.

There are clear trends in Table 5, but they are rather difficult to interpret. If we consider the *para* substituent data only: when Y = H, the aromatic interaction becomes increasingly more favourable as X becomes more electron withdrawing, but when $Y = NO_2$, the interaction becomes more favourable as X becomes more electron donating. The data were therefore analysed using Hammett substituent constants, σ_p. Straight line correlations were obtained for plots of $\Delta\Delta G$ versus σ_p for both X and Y, and these correlations can be combined into a single function, Equation (2), plotted in Figure 4a).

$$\Delta\Delta G(p\text{-X})\ [\text{kJ mol}^{-1}] = 5.2\,\sigma_X\sigma_Y - 1.9\,\sigma_X + 1.4\,\sigma_Y - 1.5 \qquad (2)$$

The correlation with σ_p shows that the variation in functional group interaction energies in Table 5 are a consequence of the change in the electrostatics of the system due to the polarising effects of the substituents. The terms in Equation (2) can be rationalised using the simple model in Figure 5. The constant, -1.5, in Equation (2) is simply a weakly attractive edge-to-face aromatic interaction in the absence of any substituents. The cross-term, $5.2\sigma_X\sigma_Y$, makes an attractive contribution to the interaction energy when the two aromatic rings are polarised in opposite senses: this can be interpreted as the interaction between the overall functional group dipoles (Figure 5b)). The other two terms can be interpreted based on local electrostatic interactions (Figure 5a)). Electron withdrawing substituents on the edge ring make the interaction more favourable, because they increase the positive charge on the edge ring hydrogens, and this increases the electrostatic interaction with the π-electron density on the face ring. Conversely, electron donating substituents on the face ring make the interaction more favourable, because they increase the π-facial electron density, and this increases the electrostatic interaction with the edge ring hydrogens.

Due to the In/Out conformational equilibrium which invalidates the $X = m\text{-}NMe_2$ double mutant cycles (Scheme 6), the only interaction energy data available from the *meta* substituted edge rings is for $X = m\text{-}NO_2$. Nevertheless, this data can be analysed in the same manner along with the data for the simple unsubstituted edge ring ($X = p$-H

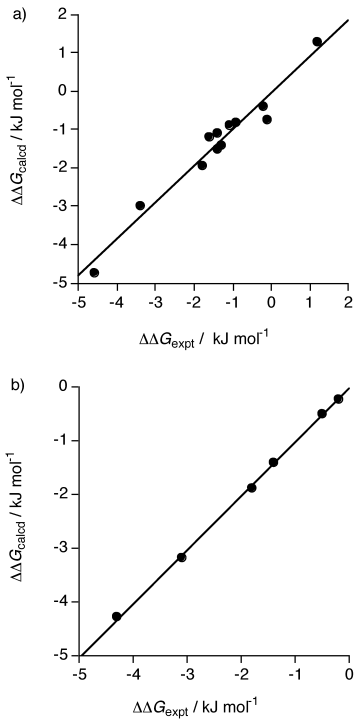

Figure 4. Hammett plots for the experimental double mutant cycle aromatic interaction energies in Table 5. a) Experimental data for the *para*-substituted edge rings plotted against the values calculated using Equation (2). b) Experimental data for the *meta*-substituted edge rings plotted against the values calculated using Equation (3). The data for *m*-NMe_2 are not shown, because these complexes adopt the In conformation (Figure 3), and this invalidates the approach.

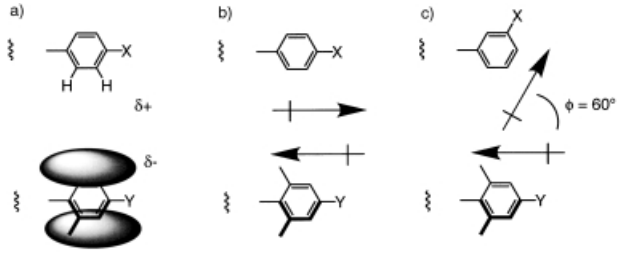

Figure 5. A model which explains the Hammett correlations in Equations (2) and (3). a) The last three terms in Equations (2) and (3) are the same, and this reflects local electrostatic interactions between the positively charged hydrogens on the edge ring and the π-electron density on the face ring. Changing the orientation of the substituent has little effect on these interactions. b) The cross-term in Equation (2) reflects the electrostatic interaction between the global dipoles across the two *para*-substituted aromatic rings. The interaction is most favourable when the two groups are polarised in opposite directions. c) The cross-term in Equation (3) also reflects the electrostatic interaction between the global dipoles across the two *meta*-substituted aromatic rings. Again, the interaction is most favourable when the two groups are polarised in opposite directions, but because the dipoles are no longer parallel, the magnitude of this effect is reduced by a factor of 2 ($1/\cos 60^\circ$).

and X = *m*-H are identical). Again straight line correlations are obtained from Hammett plots using the Y substituent constants. There are only two X substituents, but using these in the same way as before, we can derive a relationship for the *meta* substituent interaction energy as a function of the X and Y substituent constants, Equation (3), which is plotted in Figure 4b).

$$\Delta\Delta G(m\text{-X})\ [\mathrm{kJ\,mol^{-1}}] = 2.5\,\sigma_X\sigma_Y - 2.3\,\sigma_X + 1.5\,\sigma_Y - 1.4 \quad (3)$$

The coefficients in Equations (2) and (3) are very similar with the exception of the cross-term which is significantly smaller for the meta substituents. This indicates that the local electrostatic effects in Figure 5a) are insensitive to the position of the X substituent: the edge ring hydrogens are still made more positive by an electron withdrawing group. However, the global electrostatic effects are very sensitive to the position of the substituent. This can be explained, if we consider that changing from a *para* to a *meta* substituent rotates the global dipole of the edge ring through 60°, so the functional group dipoles are no longer aligned, and the interaction is reduced (compare Figure 5b) and c)). Indeed, if we assume that the dipoles are approximately parallel in the *para* case, then we should expect the dipole–dipole interaction energy to fall by a factor of $\cos 60^\circ = 0.5$ in the *meta* case. This is exactly what is observed: the cross-term coefficient in Equation (3) is half that in Equation (2). Thus, although there is significantly less data for the *meta* system, the behaviour provides good support for the explanation proposed for the *para* substituents. The *meta* data and consequently Equation (3) is affected to some extent by the assumptions about the In–Out equilibrium in Scheme 6. If the statistical factor of two was not applied in Equatiopn (1), then all of the $\Delta\Delta G$ values for X = *m*-NO_2 would be raised by 1.7 kJ mol^{-1}. Therefore the correlation with the Hammett substituent constants would be equally good, and although some of the coefficients would be altered, the coefficient for the cross-term would still be 2.5. We can thus derive a generalised Hammett equation for all of the complexes discussed here:

$$\Delta\Delta G\ [\mathrm{kJ\,mol^{-1}}] = (5.2\cos\phi)\,\sigma_X\,\sigma_Y - 0.1\,\sigma_X + 1.5\,\sigma_Y - 1.4 \quad (4)$$

where ϕ is the angle between the polarising substituents on the two aromatic rings.

Quantification of secondary interactions: As discussed above, the secondary interactions in these systems are significant. They represent the sum of changes in H-bond strength and interactions between the mutated aromatic rings and the core of the zipper complex, such as the CH–O hydrogen bond shown in Figure 2. The secondary interactions are quantified by comparing individual arms of the double-mutant cycles (Table 6). The data for the benzoyl groups can be interpreted in a straightforward manner, since the only difference between complexes C and D is the benzoyl to *tert*-butyl mutation, that is the secondary interactions are given by $\Delta G_C - \Delta G_D$ (Scheme 1). However, the data for the aniline groups is more complicated, because two functional groups are simultaneously mutated on going from B to D. The secondary interactions could be estimated as $(\Delta G_B - \Delta G_D)/2$, but this value is perturbed by a contribution from changes in the benzoyl–aniline interaction. A better measure of the secondary interactions between the aniline groups and the core of the complex alone can be obtained by considering the complexes formed with **5** (Scheme 7). The values turn out to be similar to those obtained from $(\Delta G_B - \Delta G_D)/2$ (see Table 6), but we will only discuss the data obtained using the **5** complexes.

Table 6. Secondary interactions ($\Delta\Delta G$ in kJ mol^{-1}) in deuterochloroform at 295 K.

Functional group	Position in complex A			
	Y[a]	**Y**[b]	***p*-X**[c]	***m*-X**[c]
NMe_2	$+1.2\pm0.5$	$+0.7\pm0.4$	-1.3 ± 0.3	-0.4 ± 0.4
*t*Bu	–	–	-1.0 ± 0.4	–
H	-0.4 ± 0.4	-1.3 ± 0.3	-0.9 ± 0.5	-0.9 ± 0.5
NO_2	-3.9 ± 0.3	-5.1 ± 0.3	-2.3 ± 0.4	-2.4 ± 0.4

[a] Calculated using the complexes formed with compound **5** (Scheme 7). [b] Calculated using the difference $\Delta G_B - \Delta G_D$ in Scheme 1. [c] Calculated using the difference $\Delta G_C - \Delta G_D$ in Scheme 1.

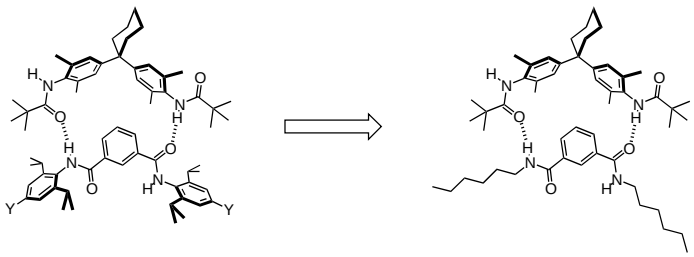

Scheme 7. Complexes used to quantify the magnitude of the secondary interactions between the substituted aniline rings and the core of the complex.

The values of the secondary interactions range from +1.2 to −2.4 kJ mol^{-1} and are plotted against σ_p in Figure 6. The data for the anilines and *meta* substituted benzoyl groups give similar correlations with σ_p: the more electron withdrawing the substituent, the more stable the complex. In these two systems, the substituents are not directly conjugated to the amide group, and so inductive effects dominate. The results can be rationalised as changes in hydrogen-bond strength due to changes in the polarity of the amide NH, although there may be additional effects such as the CH···O hydrogen bond between **k′** and the isophthaloyl amide oxygen discussed above. The behaviour of the *para* substituted benzoyl groups is similar in the electron withdrawing regime, but there is a change of slope for electron donating groups (Figure 6). In these systems, the substituent is directly conjugated to the amide group, and this may cause a change in the structure of the complex through the α–β conformational equilibrium discussed above. Electron donating groups should make the amide carbonyl oxygen a better hydrogen-bond acceptor favouring the α conformer, while electron withdrawing groups should make the amide NH a better hydrogen-bond acceptor favouring the β conformer. The changes in chemical shift confirm that the X = NO_2 systems adopt the β conformer, but the data for the electron donating substituents is less clear cut.

0947-6539/02/0813-2856 $ 20.00+.50/0 *Chem. Eur. J.* **2002**, *8*, No. 13

Improved hydrogen-bonding interactions in the α and β conformation for $X = NMe_2$ and NO_2 respectively, would explain the bell-shaped curve in Figure 6.

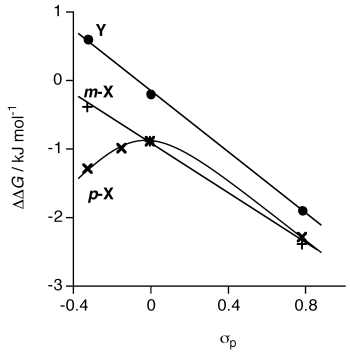

Figure 6. Hammett plot of the secondary interactions in the complexes used in the double mutant cycles (Table 6). The values for the *meta*-substituted edge ring (*m*-X) and for the face ring (Y) correlate with the Hammett substituent constants, but the curvature of the plot for the *para*-substituted edge ring (*p*-X) suggests that there is a change in structure for these complexes.

A basic assumption of the double mutant cycle approach is that the secondary interactions and changes in hydrogen-bond strength are additive functions of the mutations. However, electrostatic interactions such as hydrogen bonds are proportional to the product of the dipole moments not the sum.[9c, 15] The change in a product is only equal to the change in a sum in the limit of small net changes in dipole moment. The secondary interactions measured here are large relative to some of the aromatic interaction energies, and these experiments therefore provide a good test of the validity of the basic additivity assumption. Literature measurements of hydrogen-bond energies in chloroform give values in the range 7–8 kJ mol^{-1}.[16] The largest secondary interactions are -2.4 kJ mol^{-1} for $X = m\text{-}NO_2$ and -1.9 kJ mol^{-1} for $Y = NO_2$, and these can be attributed to increases of 32% and 25% in the size of the corresponding amide dipole moment, if we assume that all of the secondary interaction energy is due to a change in the strength of the hydrogen bond at the mutation site. The error introduced in the double mutant cycle by the additivity assumption can be evaluated as follows:

Using the double mutant cycle assumption that the secondary interactions are additive, the contribution of the hydrogen bond at the mutation site in complex D equals:

$$\approx -7.5 - 2.4 - 1.9 = -11.8 \text{ kJ mol}^{-1} \quad (5)$$

If the hydrogen-bond energy is related to the product of the dipoles (increased by 32% and 25%), the effects are multiplicative, so that the contribution of the hydrogen bond at the mutation site in complex D equals to:

$$\approx -7.5\ (1.32 \times 1.25) = -12.4 \text{ kJ mol}^{-1} \quad (6)$$

The difference between Equations (5) and (6) is 0.6 kJ mol^{-1}, and this is the maximum error introduced by our additivity assumption, since we are considering the complexes where the effects are largest. Although there are relatively large secondary interactions and changes in hydrogen-bond strength in this system, the first order perturbations are removed by the double mutant cycle, and the second-order effects are comparable with the experimental errors (0.6 kJ mol^{-1}).

Conclusion

These experiments show that electronic polarisation of π systems can have a dramatic effect on the magnitude of the non-covalent interaction between two simple aromatics. The interaction energies measured range from $+1.0$ kJ mol^{-1} repulsive to -4.9 kJ mol^{-1} attractive which represents an order of magnitude in binding affinity. The experiments show that secondary interactions caused by changes in hydrogen-bond strength are significant in these systems, but that the double-mutant approach allows these effects to be measured and removed. The results correlate well with Hammett substituent constants which indicates that the differences in interaction energy are electrostatic in origin, and a simple interpretation in terms of local and global electrostatic interactions in proposed. Limitations of the approach due to various conformational equilibria which are possible in this system have been analysed in detail, and for all but the $X = m\text{-}NMe_2$ complexes, the experimental data indicates that the effects are either small or cancel out in the double mutant cycles.

Experimental Section

The preparation of **1**–**6** have been described previously.[9] All reagents were purchased from the Aldrich Chemical Company and used without further purification.

General procedure for amide coupling reactions: The acid chloride (1 mmol) was added to a stirred solution of the amine (1 mmol) and triethylamine (1 mmol) in dry dichloromethane (15 mL). The reaction mixture was stirred for 12 h before work-up with 1M HCl (2×20 mL), 1N NaOH (2×20 mL) and brine (20 mL). After drying over anhydrous $MgSO_4$, the solvent was removed under reduced pressure. The product was passed through a silica plug with dichloromethane eluant prior to recrystallisation from dichloromethane and petroleum ether 40-60.

Compound 7: Coupling of benzoyl chloride (0.13 mL, 0.16 g, 1.15 mmol) and **6** (0.50 g, 1.05 mmol) in the presence of triethylamine (0.16 mL, 0.12 g, 1.15 mmol) gave **7** as a white powder (0.56 g, 90%). M.p. 181–183 °C; ^{1}H NMR (250 MHz, $CDCl_3$, 21 °C): $\delta = 7.90$ (d, 2H), 7.85 (d, 2H), 7.55–7.44 (m, 5H), 7.28 (s, 2H), 7.03 (s, 4H), 2.30–2.10 (br m, 16H), 1.65–1.40 (br m, 6H), 1.30 (s, 9H); ^{13}C NMR (62.5 MHz, $CDCl_3$, 21 °C): $\delta = 166.05$, 165.86, 155.17, 147.34, 135.04, 134.57, 131.37, 131.62, 128.86, 128.62, 127.42, 127.31, 127.18, 126.99, 125.60, 118.22, 45.38, 37.06, 34.98, 31.21, 26.35, 22.91, 18.85; MS (+ve, FAB): *m*/*z* (%): 587 (100) $[M+H]^+$; elemental analysis calcd (%) for $C_{42}H_{51}N_3O_2(H_2O)_{0.5}$; calcd for: C 80.63, H 7.95, N 4.70; found: C 80.54, H 7.89, N 4.66.

Compound 8: Coupling of 3-nitrobenzoyl chloride (0.17 g, 0.91 mmol) and **6** (0.44 g, 0.91 mmol) in the presence of triethylamine (0.13 mL, 0.09 g, 0.91 mmol) gave **8** as a pale yellow solid after purification by medium-pressure chromatography with ethanol/dichloromethane (1:99) and recrystallisation from dichloromethane/petroleum ether 40-60 (0.50 g, 86%). M.p. 184–186 °C; ^{1}H NMR (250 MHz, $CDCl_3$, 21 °C): $\delta = 8.71$ (s, 1H), 8.30 (d, 1H), 8.15 (d, 1H), 7.90 (s, 1H), 7.79 (d, 2H), 7.55 (t, 1H), 7.47 (d, 2H), 7.39 (s, 1H), 7.00 (s, 4H), 2.32–2.20 (br m, 4H), 2.15 (s, 6H), 2.14 (s, 6H), 1.60–1.42 (br m, 6H), 1.36 (s, 9H); ^{13}C NMR (62.5 MHz, $CDCl_3$, 21 °C): $\delta = 165.95$, 163.80, 155.31, 148.21, 148.00, 147.31, 136.13, 135.08, 134.99, 133.36, 131.54, 131.42, 130.92, 129.76, 127.09, 127.06, 126.96, 126.04, 125.63, 122.45, 31.19, 26.34, 22.90, 22.66, 18.81, 18.76; MS (+ve, FAB): *m*/*z* (%): 632 (100) $[M+H]^+$; elemental analysis calcd (%) for $C_{40}H_{45}N_3O_4(H_2O)_{0.5}$: C 74.97, H 7.24, N 6.56; found: C 74.95, H 7.06, N 6.55.

Compound 9: Coupling of 3-(dimethylamino)benzoyl chloride (0.23 g, 1.37 mmol) and **6** (0.60 g, 1.24 mmol) in the presence of triethylamine (0.19 mL, 0.14 g, 1.37 mmol) gave **9** as a white solid after purification by medium-pressure chromatography with ethanol/dicloromethane (1:99) eluant and recrystallisation from dichloromethane and petroleum ether 40-60 (0.59 g, 76%). M.p. 169–172 °C; ^{1}H NMR (250 MHz, $CDCl_3$, 21 °C): $\delta = 7.85$ (d, 2H), 7.50 (d, 2H), 7.40–7.26 (m, 4H), 7.12 (d, 1H), 7.04 (s, 4H), 6.90 (d, 1H), 3.05 (s, 6H), 2.35–2.15 (br m, 16H), 1.65–1.42 (br m, 6H), 1.35 (s, 9H); ^{13}C NMR (62.5 MHz, $CDCl_3$, 21 °C): $\delta = 166.81$, 165.95, 155.07, 150.07, 147.29, 135.45, 135.06, 131.72, 131.52, 129.22, 127.24, 126.96, 125.55, 115.40, 114.37, 111.57, 45.37, 40.52, 37.08, 34.97, 31.24, 26.40, 22.95, 18.87; MS (+ve, FAB): *m/z* (%): 630 (100) $[M+H]^+$; elemental analysis calcd (%) $C_{42}H_{51}N_3O_2(H_2O)_{0.5}$: C 78.96, H 8.20, N 6.58: found: C 79.02, H 8.06, N 6.57.

Compound 10: Coupling of 4-nitrobenzoyl chloride (0.23 g, 1.24 mmol) and **6** (0.40 g, 0.83 mmol) in the presence of triethylamine (0.18 mL, 0.13 g, 1.24 mmol) and 4-(dimethylamino)pyridine (0.01 g) gave **10** as a pale yellow solid after purification by medium-pressure chromatography with ethanol/dichloromethane (1:99) and recrystallisation from dichloromethane and petroleum ether 40-60 (0.30 g, 58%). M.p. 192–194 °C; ^{1}H NMR (250 MHz, $CDCl_3$, 21 °C): $\delta = 8.31$ (d, 2H), 8.05 (d, 2H), 7.83 (d, 2H), 7.50 (d, 2H), 7.49 (s, 1H), 7.28 (s, 1H), 7.04 (s, 2H), 7.01 (s, 2H), 2.26–2.20 (br m, 4H), 2.23 (s, 12H), 1.60–1.40 (br m, 6H), 1.31 (s, 9H); ^{13}C NMR (62.5 MHz, $CDCl_3$, 21 °C): $\delta = 165.98$, 164.21, 155.33, 149.44, 147.77, 139.92, 135.11, 135.03, 131.43, 131.11, 128.77, 127.19, 127.08, 126.93, 125.53, 123.44, 45.38, 37.04, 34.99, 31.20, 26.29, 22.89, 18.69, 18.61; MS (+ve, FAB): *m/z* (%): 632 (100) $[M+H]^+$; elemental analysis calcd (%) $C_{40}H_{45}N_3O_4(H_2O)_{0.5}$: C 74.97, H 7.24, N 6.56; found: C 74.48, H 7.14, N 6.35.

Compound 11: 4-(Dimethylamino)benzoic acid (0.044 g, 0.24 mmol) was converted to the acid chloride by stirring with oxalyl chloride (1 mL) in dry dichloromethane (10 mL) for an hour, then evaporating to dryness on a rotary evaporator followed by high vacuum. The solid residue was coupled with **6** (0.12 g, 0.24 mmol) in the presence of triethylamine (0.034 mL, 0.024 g, 0.24 mmol) gave **11** as a white solid after purification by medium-pressure chromatography with ethanol/dichloromethane (3:97) and recrystallisation from dichloromethane and petroleum ether 40-60 (0.05 g, 33%). M.p. 179–182 °C; ^{1}H NMR (250 MHz, $CDCl_3$, 21 °C): $\delta = 7.85$ (d, 2H), 7.80 (d, 2H), 7.54 (d, 2H), 7.30 (s, 1H), 7.15 (s, 1H), 7.04 (s, 2H), 7.02 (s, 2H), 6.70 (d, 2H), 3.11 (s, 6H), 2.28–2.18 (br m, 4H), 2.25 (s, 12H), 1.60–1.40 (br m, 6H), 1.37 (s, 9H); ^{13}C NMR (62.5 MHz, $CDCl_3$, 21 °C): $\delta = 165.98$, 154.91, 152.51, 147.27, 147.09, 135.16, 132.00, 131.63, 128.93, 127.35, 126.88, 125.42, 121.15, 111.03, 45.32, 40.15, 37.93, 34.93, 31.24, 26.39, 22.95, 18.80, 18.63; MS (+ve, FAB): *m/z* (%): 630 (100) $[M+H]^+$; elemental analysis calcd (%) $C_{42}H_{51}N_3O_2(H_2O)_{0.5}$: C 78.96, H 8.20, N 6.58; found: C 79.05, H 8.16, N 6.58.

Compound 14: 4-Toluene sulphonyl chloride (40.5 g, 0.21 mol) was added to a stirred solution of 2,6-diisopropylaniline (36.0 mL, 34.0 g, 0.19 mol) in dry pyridine (75 mL) and the mixture refluxed for 4 h at 146 °C. The reaction mixture was poured, with stirring, into 2 M HCl (250 mL) producing an orange/brown solution containing a pink solid which formed as the solution cooled. The solid **14** was removed by filtration and recrystallised from hot ethanol as pale pink crystals (29.40 g, 51%). M.p. 158–162 °C; ^{1}H NMR (250 MHz, [D$_6$]DMSO, 21 °C): $\delta = 9.36$ (s, 1H), 7.60 (d, 2H), 7.40 (d, 2H), 7.28 (t, 1H), 7.10 (d, 2H), 3.14 (sep, 2H), 2.35 (s, 3H), 0.95 (d, 12H); ^{13}C NMR (62.5 MHz, [D$_6$]DMSO, 21 °C): $\delta = 148.38$, 143.49, 137.43, 129.52, 128.71, 129.26, 127.41, 123.92, 28.50, 23.86, 21.51; MS (+ve, FAB): *m/z* (%): 332 (100) $[M+H]^+$.

Compound 15: Compound **14** (7.01 g, 0.021 mol), glacial acetic acid (140 mL) and sodium nitrite (2.23 g, 0.032 mol) were added successively to a stirred solution of nitric acid (30 mL) in water (140 mL). The mixture was heated at reflux for 12 h and allowed to cool to room temperature before pouring into distilled water (400 mL) whereupon the product crystallised as a white solid (5.21 g, 65%) which was collected by filtration. M.p. 149–153 °C; ^{1}H NMR (250 MHz, $CDCl_3$, 21 °C): $\delta = 8.00$ (s, 2H), 7.60 (d, 2H), 7.28 (d, 2H), 6.27 (s, 1H), 3.20 (sep, 2H), 2.44 (s, 3H), 1.06 (d, 12H); ^{13}C NMR (62.5 MHz, $CDCl_3$, 21 °C): $\delta = 150.43$, 147.80, 144.35, 136.72, 135.33, 129.82, 127.29, 119.72, 29.04, 23.56, 21.55; MS (+ve, FAB): *m/z* (%): 377 (100) $[M+H]^+$; elemental analysis calcd (%) for $C_{19}H_{24}N_2O_4S$: C 60.62, H 6.43, N 7.44, S 8.52; found: C 60.27, H 6.42, N 7.10, S 8.75.

Compound 16: Compound **15** (1.00 g, 2.91 mmol) was added to a solution of H_2SO_4/H_2O (95:5) and the mixture was stirred at room temperature for 24 h. After this time the brown solution was poured onto ice, and the mixture was made basic by the addition of NaOH pellets. The resulting yellow suspension was extracted into dichloromethane. After drying over anhydrous Na_2SO_4, solvent was removed under reduced pressure yielding a yellow solid which was recrystallised from dichloromethane/petroleum ether 40-60 (0.60 g, 93%). M.p. 105–108 °C; ^{1}H NMR (250 MHz, $CDCl_3$, 21 °C): $\delta = 7.90$ (s, 2H), 4.40 (br s, 2H), 2.80 (sep, 2H), 1.24 (d, 12H); ^{13}C NMR (62.5 MHz, $CDCl_3$, 21 °C): $\delta = 146.95$, 139.21, 131.43, 119.83, 28.02, 21.97; MS (+ve, FAB): *m/z* (%): 223 (100) $[M+H]^+$.

Compound 12: A solution of isophthaloyl dichloride (0.39 g, 1.9 mmol), **16** (0.85 g, 3.8 mmol) and 4-(dimethylamino)pyridine (0.01 g) were taken up in anhydrous pyridine (20 mL) and heated under reflux at 145 °C for 48 h. After this time, the reaction mixture was allowed to cool to room temperature and then poured into 2 M HCl in an icebath. The resulting aqueous mixture was extracted into dichloromethane (2×50 mL). The organic layers were combined, washed with brine and dried over anhydrous Na_2SO_4. The solvent was removed under reduced pressure, and the product was crystallised from hot ethanol. The white crystals **12** were filtered off and dried in vacuo (0.42 g, 38%). M.p. 318–319 °C; ^{1}H NMR (250 MHz, $CDCl_3$, 21 °C): $\delta = 8.60$ (s, 1H), 8.20 (d, 2H), 8.14 (s, 4H), 7.75 (t, 1H), 7.55 (s, 2H), 3.20 (sep, 2H), 1.30 (d, 12H); ^{13}C NMR (62.5 MHz, $CDCl_3$, 21 °C): $\delta = 166.17$, 149.15, 147.74, 139.74, 134.63, 131.25, 129.59, 127.76, 118.76, 29.10, 23.57, 23.36; MS (+ve, FAB): *m/z* (%): 575 (100) $[M+H]^+$; elemental analysis calcd (%) $C_{32}H_{38}N_4O_6(H_2O)_{0.5}$: C 65.85, H 6.56, N 9.60; found: C 65.61, H 6.54, N 9.34.

Compound 17: Compound **15** (1.42 g, 3.78 mmol) was added to a solution of anhydrous $SnCl_2$ (4.25 g, 18.9 mmol) in ethanol (20 mL) and the mixture heated at reflux (110 °C) for 90 minutes. The reaction mixture was allowed to cool to room temperature and then poured onto ice and made strongly basic by the addition of solid NaOH. The resulting yellow solution was extracted into dichloromethane and the organic layer dried over anhydrous Na_2SO_4 before removal of solvent under reduced pressure. The product **17** was isolated as a yellow solid after recrystallisation from dichloromethane and petroleum ether 40-60 (1.25 g, 96%). M.p. 186–187 °C; ^{1}H NMR (250 MHz, $CDCl_3$, 21 °C): $\delta = 7.60$ (d, 2H), 7.23 (d, 2H), 6.40 (s, 2H), 5.78 (s, 1H), 3.65 (br s, 2H), 3.05 (sep, 2H), 2.44 (s, 3H), 1.06 (d, 12H); ^{13}C NMR (62.5 MHz, $CDCl_3$, 21 °C): $\delta = 149.68$, 146.50, 143.24, 137.53, 129.42, 127.42), 120.16, 110.60, 28.38, 23.70, 21.48; MS (+ve, FAB): *m/z* (%): 347 (100) $[M+H]^+$; elemental analysis calcd (%) $C_{18}H_{26}N_2O_2S$: C 65.86, H 7.56, N 8.08, S 9.25; found: C 65.48, H 7.64, N 7.77, S 9.01.

Compound 18: A slurry of compound **17** (1.25 g, 3.62 mmol) and $NaBH_4$ (0.96 g, 25 mmol) was added dropwise to a stirred solution of 3 M H_2SO_4 (2.93 mL, 9.03 mmol) and 36% aqueous formaldehyde (1.84 mL, 22 mmol) in a conical flask keeping the temperature between −10 °C and +20 °C. When the addition was complete the mixture was made strongly basic by the addition of solid NaOH. The yellow supernatant was decanted and kept to one side and the residue remaining in the flask was treated with distilled water (20 mL) producing a grey solution which was extracted with diethyl ether. The organic solutions were combined, washed with brine and dried over anhydrous Na_2SO_4. The solvent was removed under reduced pressure yielding a yellow oil. This was crystallised from dichloromethane and petroleum ether 40-60 to give a pale yellow solid (1.09 g, 81%). M.p. 177–178 °C; ^{1}H NMR (250 MHz, $CDCl_3$, 21 °C): $\delta = 7.60$ (d, 2H), 7.23 (d, 2H), 6.40 (s, 2H), 5.85 (s, 1H), 3.10 (sep, 2H), 2.98 (s, 6H), 2.40 (s, 3H), 1.00 (d, 12H); ^{13}C NMR (62.5 MHz, $CDCl_3$, 21 °C): $\delta = 150.2$, 149.1, 143.2, 137.7, 129.4, 127.4, 118.5, 40.5, 28.6, 23.8, 21.5; MS (+ve, FAB): *m/z* (%): 374 (100) $[M]^+$.

Compound 19: Compound **18** (1.09 g, 2.91 mmol) was added to a solution of H_2SO_4/H_2O (95:5) and the mixture warmed gently at 40 °C for 6 h. After this time the brown solution was poured onto ice and the mixture made basic by the addition of NaOH pellets. The solution was extracted into dichloromethane and dried over anhydrous Na_2SO_4 before removal of the solvent under reduced pressure yielding a purple oil which was dried under high vacuum for 1 h. Thin-layer chromatography showed the presence of a trace impurity which was removed at the next step without characterisation (0.52 g, 81%). M.p. 164–166 °C; ^{1}H NMR (250 MHz, $CDCl_3$, 21 °C): $\delta = 6.65$ (s, 2H), 3.75 (br s, 2H), 3.00 (sep, 2H), 2.90 (s, 6H), 1.24 (d, 12H); ^{13}C NMR (62.5 MHz, $CDCl_3$, 21 °C): $\delta = 144.7$, 134.0, 132.4, 101.1, 42.5, 28.3, 22.6; MS (+ve, FAB): *m/z* (%): 220 (100) $[M]^+$.

  0947-6539/02/0813-2858 $ 20.00+.50/0 *Chem. Eur. J.* **2002**, *8*, No. 13

Compound 13: A solution of isophthaloyl dichloride (0.19 g, 0.95 mmol) in dry dichloromethane (10 mL) was added to a stirred solution of compound **19** (0.42 g, 1.9 mmol) and triethylamine (0.27 mL, 0.19 g, 1.9 mmol) in dry dichloromethane and the mixture was stirred for 12 h. Following work-up with 1N *ff* NaOH, brine and drying over anhydrous Na_2SO_4, the solvent was removed under reduced pressure. The product **13** was isolated as a pale brown powder after recrystallisation from dichloromethane and petroleum ether 40-60 (0.42 g, 78%). M.p. 265–267 °C; ^{1}H NMR (250 MHz, $CDCl_3$, 21 °C): $\delta = 8.50$ (s, 1H), 8.10 (d, 2H), 7.65 (t, 1H), 7.35 (s, 2H), 6.57 (s, 4H), 3.10 (sep, 2H), 2.98 (s, 12H), 1.24 (d, 12H); ^{13}C NMR (62.5 MHz, $CDCl_3$, 21 °C): $\delta = 166.69$, 150.58, 146.85, 135.30, 130.26, 129.21, 126.00, 120.50, 107.86, 40.82, 29.17, 23.81; MS (+ve, FAB): *m/z* (%): 571 (100) $[M+H]^+$; elemental analysis calcd (%) for $C_{36}H_{50}N_4O_2(H_2O)_{0.5}$: C 74.57, H 8.69, N 9.66; found: C 74.86, H 8.58, N 9.41.

NMR binding experiments: ^{1}H NMR dilution experiments were used to check whether dimerisation of compounds **1**–**7** was significant at the concentrations. All dimerisation constants are less than $5\,M^{-1}$ and so do not affect the titrations to any extent. A 3.0 mL sample of host of known concentration (2–5 mM) was prepared in $CDCl_3$. 0.8 mL of this solution was removed, and a ^{1}H NMR spectrum was recorded. An accurately weighed sample of the guest was then dissolved in the remaining 2.2 mL of host solution. This solution was almost saturated with guest (100–200 mM) to allow access as much of the binding isotherm as possible (50–80% saturation was achieved) and contained host so that the host concentration remained constant during the titration. Aliquots of guest solution were added successively to the NMR tube containing the host solution, the tube was shaken to mix the host and guest solutions, and the ^{1}H NMR spectra were recorded after each addition. For signals that moved more than 0.01 ppm, the chemical shifts at all concentrations of guest were recorded and analysed using purpose-written software on an Apple Macintosh microcomputer, NMRTit HG.[9a] This programme fits the data to a 1:1 binding model to yield the association constant, the bound chemical shifts in the HG complex, and if required, the free chemical shifts of the unbound species. All titrations were repeated at least three times, and where possible, the identities of the host and guest were reversed in order to obtain accurate $\Delta\delta$ values for both binding partners. Where this was not possible, the binding constant determined by fitting the host signals was fixed, and *NMRTit HG* was used analyse the changes in the guest signals to extract the bound guest chemical shift. The mean association constant for each experiment was evaluated as the weighted mean (based on the observed change in chemical shift) of the association constants for the individual signals monitored. The error was taken as twice the standard error. The values of K_a quoted in Table 1 are the average values and errors from at least three separate experiments. Two-dimensional ROESY spectra were recorded on a Bruker AMX2-400 using a 300 ms mixing time and a 3 s delay between pulses.

Acknowledgement

We thank the EPSRC (F.J.C.), the University of Sheffield (J.F.M.), Merck Sharp and Dohme (F.J.C.), SmithKline Beecham (J.F.M.), and the Lister Institute (C.A.H.) for financial support.

[1] a) R. E. Sheridan, H. W. Whitlock, *J. Am. Chem. Soc.* **1988**, *110*, 4071–4073; b) B. J. Whitlock, H. W. Whitlock, *J. Am. Chem. Soc.* **1990**, *112*, 3910–3915; c) T. J. Shepodd, M. A. Petti, D. A. Dougherty, *J. Am. Chem. Soc.* **1988**, *110*, 1983–1985; d) A. W. Schwabacher, S. Zhang, W. Davy, *J. Am. Chem. Soc.* **1993**, *115*, 6995–6996; e) H. J. Schneider, T. Blatter, S. Simova, I. Theis, *Chem. Commun.* **1989**, 580–581; f) A. D. Hamilton, D. Van Engen, *J. Am. Chem. Soc.* **1987**, *109*, 5035–5036; g) A. V. Muehldorf, D. Van Engen, J. C. Warner, A. D. Hamilton, *J. Am. Chem. Soc.* **1988**, *110*, 6561–6562; h) J. Rebek, D. Nemeth, *J. Am. Chem. Soc.* **1986**, *108*, 5637–5638; i) J. Rebek, B. Askew, P. Ballester, C. Buhr, S. Jones, D. Nemeth, K. Williams, *J. Am. Chem. Soc.* **1987**, *109*, 5033–5035; j) S. C. Zimmerman, C. M. Vanzyl, *J. Am. Chem. Soc.* **1987**, *109*, 7894–7896; k) S. C. Zimmerman, C. M. Vanzyl, G. S. Hamilton, *J. Am. Chem. Soc.* **1989**, *111*, 1373–1381; l) , J. N. H. Reek, A. H. Priem, H. Engelkamp, A. E. Rowan, J. Elemans, R. J. M. Nolte, *J. Am. Chem. Soc.* **1997**, *119*, 9956–9964; m) A. S. Shetty, J. S. Zhang, J. S. Moore, *J. Am. Chem. Soc.* **1996**, *118*, 1019–1027; n) L. F. Newcomb, S. H. Gellman, *J. Am. Chem. Soc.* **1994**, *116*, 4993–4994; o) N. J. Heaton, P. Bello, B. Herrandon, A. del Campo, J. Jimenez-Barbero, *J. Am. Chem. Soc.* **1998**, *120*, 12371–12384; p) G. A. Breault, C. A. Hunter, P. C. Mayers, *J. Am. Chem. Soc.* **1998**, *120*, 3402–3410; q) W. B. Jennings, B. M. Farrell, J. F. Malone, *Acc. Chem. Res.* **2001**, *34*, 885–894.

[2] G. A. Jeffrey, *An Introduction to Hydrogen Bonding*, Oxford University Press, Oxford, **1997**.

[3] C. A. Hunter, J. K. M. Sanders, *J. Am. Chem. Soc.* **1990**, *112*, 5525–5534.

[4] a) S. B. Ferguson, F. Diederich, *Angew. Chem.* **1986**, *98*, 1127–1129; *Angew. Chem. Int. Ed. Engl.* **1986**, *25*, 1127–1129; b) D. B. Smithrud, F. Diederich, *J. Am. Chem. Soc.* **1990**, *112*, 339–343.

[5] a) F. Cozzi, M. Cinquini, R. Annunziata, T. Dwyer, J. S. Siegel, *J. Am. Chem. Soc.* **1992**, *114*, 5729–5733; b) F. Cozzi, M. Cinquini, R. Annunziata, J. S. Siegel, *J. Am. Chem. Soc.* **1993**, *115*, 5330–5331.

[6] F. Cozzi, F. Ponzini, R. Annunziata, M. Cinquini, J. S. Siegel, *Angew. Chem.* **1995**, *107*, 1092–1093; *Angew. Chem. Int. Ed. Engl.* **1995**, *34*, 1019–1020.

[7] a) S. Paliwal, S. Geib, C. S. Wilcox, *J. Am. Chem. Soc.* **1994**, *116*, 4497–4498; b) E. Kim, S. Paliwal, C. S. Wilcox, *J. Am. Chem. Soc.* **1998**, *120*, 11192–11193.

[8] a) H. Adams, F. J. Carver, C. A. Hunter, J. C. Morales, E. M. Seward, *Angew. Chem.* **1996**, *108*, 1628–1631; *Angew. Chem. Int. Ed. Engl.* **1996**, *35*, 1542–1544; b) H. Adams, K. D. M. Harris, G. A. Hembury, C. A. Hunter, D. Livingstone, J. F. McCabe, *J. Chem. Soc. Chem. Commun.* **1996**, 2531–2532; c) F. J. Carver, C. A. Hunter, E. M. Seward, *Chem. Commun.* **1998**, 775–776.

[9] a) A. P. Bisson, C. A. Hunter, J. C. Morales, K. Young, *Chem. Eur. J.* **1998**, *4*, 845–851; b) A. P. Bisson, F. J. Carver, D. S. Eggleston, R. C. Haltiwanger, C. A. Hunter, D. L. Livingstone, J. F. McCabe, C. Rotger, A. E. Rowan, *J. Am. Chem. Soc.* **2000**, *122*, 8856–8868; c) F. J. Carver, C. A. Hunter, P. S. Jones, D. J. Livingstone, J. M. McCabe, E. M. Seward, P. Tiger, S. E. Spey, *Chem. Eur. J.* **2001**, *7*, 4854–4862.

[10] a) B. M. Wepster, *Rec. Trav. Chim.* **1953**, *73*, 809–818; b) B. M. Wepster, *Rec. Trav. Chim.* **1957**, *76*, 357–389; c) G. Chiavari, A. G. Giumanini, M. M. Musiani, P. Rossi, *Synthesis* **1980**, 743–746.

[11] K. A. Connors, *Binding Constants*, Wiley, Chichester, **1987**.

[12] M. J. Packer, C. A. Hunter, *Chem. Eur. J.* **1999**, *5*, 1891–1897.

[13] In all of the complexes illustrated the amide groups are oriented *trans* across the isophthaloyl and bisaniline units, so that each molecules features one H-bond donor and one H-bond acceptor. This geometry is the lowest energy conformation from molecular mechanics calculations and NMR structure determination.[12] Nevertheless, it is possible that one or both of the amide *cis* conformations are populated to some extent. When $Y = NO_2$, the bisaniline **NH** and **NH′** $\Delta\delta$ values are lower than in the other complexes, and there is an increase in the $\Delta\delta$ value of the isophthaloyl **NH** signal which is suggestive of a *cis* conformation, where the isophthaloyl amides are both H-bond acceptors. However, this would pull the isophthaloyl group out of the bisaniline pocket significantly changing the $\Delta\delta$ values for **a** and **b**. The pattern of chemical shift changes in the rest of the complex does not alter when $Y = NO_2$ suggesting that electric field effects are probably responsible for the differences in amide chemical shift. In any case, structural changes when $Y = NO_2$ will be manifest in both complexes A and C, so the thermodynamic consequences will cancel out in the double-mutant cycle.

[14] H. Adams, P. L. Bernad, D. S. Eggleston, R. C. Haltiwanger, K. D. M. Harris, G. A. Hembury, C. A. Hunter, D. J. Livingstone, B. M. Kariuki, J. F. McCabe, *Chem. Commun.* **2001**, 1500–1501.

[15] M. Herail, E. Megnassan, A. Proutiere, *J. Phys. Org. Chem.* **1997**, *10*, 167–174.

[16] The precise value used for a H-bond does significantly affect this analysis, but 7.5 kJ mol^{-1} seems to be a reasonable estimate. a) Y. Aoyama, A. Yamagishi, M. Asagawa, H. Toi, H. Ogoshi, *J. Am. Chem. Soc.* **1988**, *110*, 4076–4077; b) S.-K. Chang, D. Van Engen, E. Fan, A. D. Hamilton, *J. Am. Chem. Soc.* **1991**, *113*, 7640–7645.

Received: November 6, 2001 [F3664]